

Alterations of Microstructure and Sodium Homeostasis in Fast Amyotrophic Lateral Sclerosis Progressors: A Brain DTI and Sodium MRI Study

M.M. El Mendili, A.-M. Grapperon, R. Dintrich, J.-P Stellmann, J.-P. Ranjeva, M. Guye, A. Verschueren, S. Attarian, W. Zaaraoui

▶ **To cite this version:**

M.M. El Mendili, A.-M. Grapperon, R. Dintrich, J.-P Stellmann, J.-P. Ranjeva, et al.. Alterations of Microstructure and Sodium Homeostasis in Fast Amyotrophic Lateral Sclerosis Progressors: A Brain DTI and Sodium MRI Study. American Journal of Neuroradiology, 2022, 43 (7), pp.984-990. 10.3174/ajnr.A7559 . hal-03772234

HAL Id: hal-03772234
https://amu.hal.science/hal-03772234

Submitted on 14 Nov 2022

HAL is a multi-disciplinary open access archive for the deposit and dissemination of scientific research documents, whether they are published or not. The documents may come from teaching and research institutions in France or abroad, or from public or private research centers.

L'archive ouverte pluridisciplinaire **HAL**, est destinée au dépôt et à la diffusion de documents scientifiques de niveau recherche, publiés ou non, émanant des établissements d'enseignement et de recherche français ou étrangers, des laboratoires publics ou privés.



Distributed under a Creative Commons Attribution 4.0 International License

Title: Alterations of Microstructure and Sodium Homeostasis in Fast Amyotrophic Lateral Sclerosis Progressors: A Brain DTI and Sodium MRI Study

Authors: Mohamed Mounir EL MENDILI[1,2], PhD, Aude-Marie GRAPPERON[1,2,3], MD, Rémi DINTRICH[1,2,3], MSc, Jan Patrick STELLMANN[1,2], MD, Jean-Philippe RANJEVA[1,2], PhD, Maxime GUYE[1,2], MD, PhD, Annie VERSCHUEREN[1,2,3], MD, Shahram ATTARIAN[3], MD, PhD, Wafaa ZAARAOUI[1,2], PhD

Affiliations:

[1]Aix Marseille Univ, CNRS, CRMBM, Marseille, France

[2]APHM, Hopital de la Timone, CEMEREM, Marseille, France

[3]APHM, Hôpital de la Timone, Referral Centre for Neuromuscular Diseases and ALS, Marseille, France

Corresponding Author:

Mohamed Mounir EL MENDILI

Centre de Résonance Magnétique Biologique et Médicale, CRMBM-CEMEREM, UMR 7339 CNRS - Aix–Marseille Université, 27 Bd Jean Moulin, 13005 Marseille, France.

E-mail: mm.elmendili@univ-amu.fr

Phone: +33 (0)4 91 38 84 66

Fax: +33 (0)4 91 38 84 61

Funding: This research was funded by APHM (AORC Junior 2014 program), ARSLA (Association pour la Recherche sur la Sclérose Latérale Amyotrophique et autres maladies du motoneurone) and FRC (Fédération pour la Recherche sur le Cerveau).

ABSTRACT

BACKGROUND AND PURPOSE

While conventional MRI has limited value in amyotrophic lateral sclerosis (ALS), non-conventional MRI has shown alterations of microstructure using diffusion MRI and recently sodium homeostasis with sodium MRI.

We aimed to investigate the topography of brain regions showing combined microstructural and sodium homeostasis alterations in ALS subgroups according to their disease progression rates.

MATERIALS AND METHODS

Twenty-nine patients with ALS and 24 age-matched healthy controls (HC) were recruited. Clinical assessments included disease duration and the revised ALS functional rating scale (ALSFRS-R). Patients were clinically differentiated into fast (n=13) and slow (n=16) progressors according to their ALFSRS-R progression rate.

3T MRI brain protocol included: (1) ^{1}H T1-weighted and diffusion sequence; (2) ^{23}Na density-adapted radial sequence. Quantitative maps of diffusion with fraction anisotropy (FA), mean diffusivity (MD) and total sodium concentration (TSC) were measured. The topography of diffusion and sodium abnormalities were assessed by voxel-wise analyses.

RESULTS

ALS patients showed significantly higher TSC and lower FA, alongside higher TSC and higher MD, compared to HC, primarily within the corticospinal tracts (CSTs), the corona radiata and the body and genu of the corpus callosum. Fast progressors showed wider spread abnormalities mainly in frontal areas. In slow progressors, only FA measures showed abnormalities when compared to HC, localized in focal regions of the CSTs, the body of corpus callosum, the corona radiata and the thalamic radiation.

CONCLUSION

The present study evidenced widespread combined microstructural and sodium homeostasis brain alterations in fast ALS progressors.

INTRODUCTION

Amyotrophic lateral sclerosis (ALS) is a relentlessly progressive neurodegenerative disorder leading to paralysis and ultimately death. As a heterogeneous condition, ALS is characterized by variable clinical presentations and progressions of symptoms depending on various factors such as age at disease onset, the site of onset, genetic factors, and the presence of non-motor symptoms, especially cognitive impairment.[1-4] ALS outcome drastically varies, with a median survival time from onset ranging from 24 months (North Europe) to 48 months (South Asia).[5] For 1.1% of ALS cases, the median survival time from onset is 18 months and can go up to 10 years in 5 to 13.3% of cases, demonstrating the heterogeneity of the disease.[3,6] While disability is commonly scored by the ALS functional rating scale (ALSFRS-R), the ALSFRS disease progression rate is also considered as an important marker of the disease to predict disability progression and patient survival.[7-9]

Conventional MRI (e.g. $T2^*$, fluid-attenuated inversion recovery and proton density-weighted imaging) lacks sensitivity and specificity to detect abnormalities in ALS and is mainly used to exclude ALS-mimics.[10] Although conventional MRI could detect abnormal signal in ALS such as hyperintensity in the white matter along the corticospinal tract (CST), they are rare, nonspecific, and their exploration is not recommended for diagnosis.[10-13] In contrast, non-conventional MRI has gradually characterized features of neurodegeneration in ALS.[14] To a large extent, diffusion tensor imaging (DTI) studies have reported microstructure alterations in upper-motor neurons and extra-motor white matter tracts.[15] Notably, DTI has shown increased burdens of white matter pathology, concordant with neuropathological staging and correlating with disease aggressiveness.[14,16-18] Recently, a sodium MRI study provided the first evidence of increased total sodium concentration (TSC) located in the CST of ALS patients, reflecting sodium homeostasis disturbance involved in metabolic failure contributing to the neurodegenerative process.[19] Mitochondrial dysfunction can mediate cell death by reducing ATP production and impairing sodium and calcium homeostasis. If ATP availability becomes insufficient to allow ion pumps to maintain the appropriate ion gradients, changes in electrical properties and excitability of motor neurons occur. Thus, investigating sodium concentration disturbances with sodium MRI could provide relevant functional information on neuron energetic status and cell viability while DTI explores efficiently microstructural disorders. The combination of sodium and diffusion imaging could therefore enable

the exploration of complementary processes leading to neuronal injury. Besides, one may assume that brain regions presenting combined sodium homeostasis and microstructural alterations depends on disease aggressiveness. The present study aimed at investigating the topography of brain regions showing combined microstructural and sodium homeostasis alterations in ALS subgroups according to their disease progression rates.

MATERIALS AND METHODS

Ethics and Institutional Review Board Approval

This prospective study was approved by the local ethics committee, and written informed consent was obtained from all participants.

Study Participants and study procedures

Twenty-nine patients with ALS (9 females, mean age ± SD: 54 ± 10 years old, mean disease duration ± SD: 1.6 ± 1.2 years) were recruited from the ALS reference center of our university hospital and 24 age and sex-matched healthy controls (HC) with no history of neurologic or neuropsychiatric disorder (11 females, age 51 ± 11 years old). The inclusion criteria were a diagnosis of ALS according to the revised El Escorial criteria.[20] The exclusion criteria were no current or past history of neurologic disease other than ALS, and no frontotemporal dementia, respiratory insufficiency, or substantial bulbar impairment incompatible with an MRI examination. Patients were clinically assessed immediately after the MRI and scored on the revised ALS Functional Rating Scale (ALSFRS-R).[21] Patients were clinically differentiated into fast and slow progressors according to their ALFSRS-R rate of progression, defined as ([48 - ALSFRS-R] / disease duration). A threshold of 0.5 ALSFRS-R per month was set to differentiate fast from slow progressors.[22]

MRI acquisition

MRI acquisition was performed on a 3T Verio system (Siemens, Erlangen, Germany) using a 32-channel phased-array ^{1}H head coil (Siemens) and a ^{23}Na-^{1}H volume head coil (Rapid Biomedical).

^{1}H MRI protocol included a 3D T1-weighted (T1w) Magnetization-Prepared Rapid Acquisition Gradient-Echo (MPRAGE) sequence (TE/TR/TI = 3/2300/900 ms, 160 slices, voxel size = 1×1×1 mm^3, acquisition time = 6 min), and a single shot echo-planar imaging DTI sequence (64 encoding directions, b = 1000 s/mm^2 and a b0, TE = 95 ms, TR = 10700 ms, 60 contiguous slices, voxel size = 2×2×2 mm^3, acquisition time = 12 min).

^{23}Na MRI protocol included a 3D density-adapted radial sequence (TR/TE = 120/0.2 ms; 17000 projections with 369 samples per projection; voxel size = 3.6×3.6×3.6 mm^3; acquisition time = 34 min).[23] Two tubes (50 mmol/L within 2% of agar gel) placed within the FOV served as a reference for quantification.[24]

Data processing

Anatomical. T1w images were normalized to the Montreal National Institute 152 template (MNI152) using SyN-ANTS non-linear registration.[25]

Diffusion tensor imaging. Diffusion images were denoised using a Local Principal Component Analysis method that reduces signal fluctuations solely rooted in thermal noise.[26] Images were further corrected for eddy currents and head motion using affine registration to the associated non-diffusion-weighted images.[27] Fractional anisotropy (FA), mean diffusivity (MD), axial diffusivity (AD), and radial diffusivity (RD) maps were computed by fitting a tensor model.[27] FA images were aligned to the FMRIB58_FA target which is in MNI152 standard space using a non-linear registration.[27] Aligned FA images were averaged, then a "thinning" (non-maximum-suppression perpendicular to the local tract structure) was applied to create a skeletonized mean FA image. The resulting image was thresholded (FA = 0.2) to suppress areas of low mean FA and/or high inter-subject variability.[28] For each subject's FA image, the maximum FA value perpendicular to each voxel of the skeleton was projected onto the mean FA skeleton. Similarly, skeletonized MD, AD and RD images were generated in the MNI152 space using TBSS-FSL tools, prior to voxel-wise analysis.

Sodium imaging. Sodium images were reconstructed offline, denoised, and then normalized relative to the reference tube signals to compute quantitative TSC maps of the whole brain.[19,24] TSC maps were rigidly aligned to their corresponding T1w image. Linear and non-linear transformations were concatenated then used

to bring TSC maps into the MNI152 standard space and spatially normalized TSC maps were smoothed with a Gaussian kernel (8 × 8 × 8 mm) prior to voxel-wise analysis.

Statistical analysis

Statistical analysis was performed using FSL (FMRIB Software Library v6.0)[27] and Statistical Package for Social Science (SPSS v23, IBM corp.).

Group comparisons. Differences for age, disease duration (DD) and the ALSFRS-R score between groups were assessed using Student's t-test or the Kruskal-Wallis test, when applicable. Differences for gender between groups were assessed using the Chi-squared test.

Voxel-wise analysis. Differences in diffusion (FA, MD, RD, AD) and sodium (TSC) maps between groups (ALS patients vs HC; fast vs HC; slow vs HC; fast vs slow) were assessed using permutation inference statistics (5000 permutations), combined with t-testing. Threshold-free cluster enhancement (TFCE) with a significance interval of p-values < 0.05 was used to correct for multiple comparisons (i.e. family-wise error correction).[28] Common regions with significant group differences in both diffusion and TSC maps were identified from the Johns Hopkins University WM tractography atlas and labels, and the Harvard-Oxford structural atlas and sorted by overlap with the corresponding tracts, cortical and subcortical regions.

RESULTS

Demographical and clinical measures of our population are reported in Table 1. Figure 1 shows an example of FA and TSC images in a HC, fast and slow progressor patients. There were no significant differences in age, nor in gender between ALS, fast and slow progressor patients and HC (all p-values < 0.05). There was no significant difference in disease duration, or in ALSFRS-R between fast and slow progressors. Disease progression rate was 1.54 ± 0.93 (mean $\pm$ SD) ALSFRS-R per month for fast progressors and 0.27 ± 0.09 (mean $\pm$ SD) ALSFRS-R per month for slow progressors patients.

ALS vs HC

Statistical maps resulting from voxel-wise analysis and tract-based spatial statistics comparing ALS patients to HC for TSC, FA and MD are presented in Figure 2.

TSC. ALS patients showed significantly higher TSC compared to HC mainly at the level of the body and genu of the corpus callosum, CSTs, bilateral corona radiata and thalamic radiation for white matter, and middle frontal, precentral, postcentral and cingulate gyri and anterior division for grey matter. These clusters had a TSC of 58.15 ± 4.54 mM (mean ± SD) in ALS patients and 53.41 ± 3.22 in HC. No clusters of significantly lower TSC in ALS compared to HC were found.

DTI. ALS patients showed significantly lower FA compared to HC mainly at the level of the bilateral corona radiata, body of the corpus callosum, forceps minor, genu of corpus callosum and CSTs. ALS patients showed significantly higher MD compared to HC mainly at the level of the bilateral corona radiata, body of the corpus callosum, CSTs, internal and external capsule and longitudinal fasciculus. No clusters of significantly higher FA or lower MD in ALS compared to HC were found.

Overlap between TSC and DTI. As reported in Figure 2, compared to HC, ALS patients showed significantly higher TSC and lower FA, higher TSC and higher MD, mainly at the level of the corpus callosum, CSTs and bilateral corona radiata. No clusters of significantly higher FA and lower TSC or lower TSC and lower MD in ALS compared to HC were found. A complete list of the significant clusters emerging from the voxel-wise analysis is reported in Supplementary Table 1.

Fast versus HC

Statistical maps resulting from voxel-wise analysis comparing fast ALS progressors to HC for TSC, FA and MD are presented in Figure 3.

TSC. Fast progressors showed significantly higher TSC compared to HC mainly at the level of the body and genu of the corpus callosum, thalamic radiation, bilateral corona radiata, forceps minor and CSTs for white matter, and precentral, postcentral, cingulate, precingulate, middle frontal, superior frontal gyri, thalamus and caudate for grey and deep grey matter (Figure 3). These clusters had a TSC of 59.23 ± 5.03mM (mean ± SD)

in fast progressors and 53.12 ± 3.12 in HC. No clusters of significantly lower TSC in fast progressors compared to HC were found.

DTI. Fast progressors showed significantly lower FA compared to HC mainly at the level of the bilateral corona radiata, body and genu of the corpus callosum, forceps minor, external capsule, uncinate fasciculus and CSTs (Figure 3). Fast progressors showed significantly higher MD compared to HC mainly at the level of the bilateral corona radiata, body and genu of the corpus callosum, forceps minor, CSTs, internal capsule, longitudinal fasciculus, fronto-occipital fasciculus, thalamic radiation and external capsule (Figure 3). No clusters of significantly higher FA or lower MD in fast progressors compared to HC were found.

Overlap between TSC and DTI. As reported in Figure 3, compared to HC, fast progressors showed significantly higher TSC and lower FA, higher TSC and higher MD, mainly at the level of the corona radiata, body and genu of the corpus callosum, forceps minor and CSTs. No clusters of significantly higher FA and lower TSC or lower TSC and lower MD in fast progressors compared to HC were found. A complete list of the significant clusters emerging from the voxel-wise analysis is reported in Supplementary Table 1.

Slow versus HC

Only FA showed significantly lower values in slow progressors compared to HC mainly at the level of the bilateral superior corona radiata, CSTs, body of the corpus callosum and thalamic radiation (Figure 4). A complete list of the significant clusters emerging from TBSS analysis is reported in Supplementary Table 1.

Fast versus slow

No significant differences in TSC and DTI metrics were found between fast and slow progressors.

Results from TBSS analysis for RD and AD are reported in Supplementary Table 1 and Supplementary Figures 1 and 2.

DISCUSSION

The present study highlighted brain regions with combined microstructural and sodium homeostasis disturbances corresponding to clinically relevant regions involved in ALS, namely, the CST and the corpus callosum.[29] We opted for a whole brain voxel-to-voxel analyses to highlight the focal tissue involvement that would be masked by a global approach such as regions of interest. Our results are in accordance with DTI studies that confirmed the impairment of the CST (subcortical to brainstem) as a main hallmark in ALS, even in patients with no upper motor neuron signs at the time of MRI but who developed pyramidal symptoms later.[16,30,31] Furthermore, callosal impairment has also been stressed by several studies, especially the motor-related regions of the corpus callosum.[10,32] A recent meta-analysis DTI study analyzing 14 studies with 396 ALS patients exhibited two clusters of brain microstructural impairment.[33] The first cluster was located in the left corona radiata, extending to the body and splenium of the corpus callosum, left superior longitudinal fasciculus, posterior limb of the internal capsule, right corona radiata, and bilateral cingulate gyrus. The second cluster was located in the right corticospinal tract that extended to the right cerebral peduncle. Interestingly, these two clusters were found in our study to be the site of microstructural impairment but also sodium homeostasis disturbances, a marker of neurodegeneration related to mitochondrial dysfunction and energy failure.[19-34]

Considering that heterogeneous disease progression rates impact prognosis and might affect the responsiveness to future treatments, recent efforts have tried to study patient stratification.[35,36] Stratifying patients by disease progression, we characterized widespread combined microstructural and ionic alterations in fast progressors while slow progressors only showed restricted microstructure damage. These results are of importance as they reflect diverse pathophysiological processes in patients with no difference in age or disease duration neither disability scale (ALSFRS-R), but who experienced different disease progression rates. Few studies have investigated white matter and grey matter alterations in fast and slow progressors.[16,17,30] A DTI study reported that lower motor neuron ALS fast progressors had a substantial impairment in the CST, frontal and prefrontal brain regions compared to HC, while slow progressors showed less severe alterations.[17] In addition, high disease aggressiveness patients showed a distinct pattern of supratentorial white matter density decreases relative to those with low aggressiveness but no significant differences in grey matter density suggesting axonal

loss.[30] In our study, we found sodium alterations which reflect mitochondrial dysfunction and subsequent energy failure, both of which are key factors in the induction of pathological processes in ALS.[37,38] In vitro experiments demonstrated that axonal degeneration caused by experimental anoxia within the brain is a $Ca2^{+}$ dependent process that can be triggered by a sustained Na+ influx driving reverse Na^{+}–$Ca2^{+}$ exchange and importing damaging levels of Ca2+ within the axons.[39] This early work suggested that ATP depletion and consequent Na^{+}-K^{+}-ATPase failure might result in breakdown of ionic gradients because Na^{+} ions enter the axon via persistently activated Na+ channels. An additional study reported that axons may degenerate because nitric oxide (NO) can inhibit mitochondrial respiration resulting in energy failure and intra-axonal accumulation of sodium. Interestingly, axons could be protected from NO-mediated damage using Na^{+} channel blockers.[40]

Limitations

The cross-sectional design of the study did not allow us to assess the course of the disease between fast and slow progressors and investigate whether fast progressors are an ALS phenotype, as suggested in some studies,[16,17] or a mal-adaptative condition. In the present study, fast and slow progressors were differentiated using a threshold of 0.47 for disease progression rate. This choice was based on the results of a previous study,[22] which found that this threshold was a significant predictor of survival in ALS. Nevertheless, as no consensus is available, this choice may be open to discussion. Another limitation is related to the restricted number of patients which prevented better staging between subgroups and might explain the lack of significant difference between fast and slow progressors. Finally, a neuropsychological assessment would have helped to explain if clusters found in the frontotemporal lobe of fast progressors were due to cognitive deficits. Future multi-centric and longitudinal imaging studies will be of interest to identify early markers of neurodegeneration and predict the course of the disease of individual patients.[41]

Conclusion

The present brain DTI and sodium MRI study evidenced combined microstructural and sodium homeostasis alterations in ALS. These alterations were in accordance with disease aggressiveness. Fast progressors showed a more widespread brain tissues damage than slow progressors when compared to healthy controls. Our study

highlights the pertinence of a multinuclear MRI approach to stratify patients according to their disease aggressiveness.

REFERENCES

1- Chiò A, Moglia C, Canosa A, et al. Cognitive impairment across ALS clinical stages in a population-based cohort. Neurology. 2019 Sep 3;93(10):e984-e994. DOI: 10.1212/WNL.0000000000008063.

2- Chiò A, Logroscino G, Traynor BJ, et al. Global epidemiology of amyotrophic lateral sclerosis: a systematic review of the published literature. Neuroepidemiology. 2013;41(2):118-30. DOI: 10.1159/000351153.

3- Chiò A, Calvo A, Moglia C, et al. Phenotypic heterogeneity of amyotrophic lateral sclerosis: a population based study. J Neurol Neurosurg Psychiatry. 2011 Jul;82(7):740-6. DOI: 10.1136/jnnp.2010.235952.

4- Volk AE, Weishaupt JH, Andersen PM, et al. Current knowledge and recent insights into the genetic basis of amyotrophic lateral sclerosis. Med Genet. 2018;30(2):252-258. DOI: 10.1007/s11825-018-0185-3.

5- Marin B, Boumédiene F, Logroscino G, et al. Variation in worldwide incidence of amyotrophic lateral sclerosis: a meta-analysis. Int J Epidemiol. 2017 Feb 1;46(1):57-74. DOI: 10.1093/ije/dyw061.

6- Pupillo E, Messina P, Logroscino G, et al. Long-term survival in amyotrophic lateral sclerosis: a population-based study. Ann Neurol. 2014 Feb;75(2):287-97. DOI: 10.1002/ana.24096.

7- Kimura F, Fujimura C, Ishida S, et al. Progression rate of ALSFRS-R at time of diagnosis predicts survival time in ALS. Neurology. 2006 Jan 24;66(2):265-7. DOI: 10.1212/01.wnl.0000194316.91908.8a.

8- Kollewe K, Mauss U, Krampfl K, et al. ALSFRS-R score and its ratio: a useful predictor for ALS-progression. J Neurol Sci. 2008 Dec 15;275(1-2):69-73. DOI: 10.1016/j.jns.2008.07.016.

9- Daghlas SA, Govindarajan R; Pooled Resource Open-Access ALS Clinical Trials Consortium. Relative effects of forced vital capacity and ALSFRS-R on survival in ALS. Muscle Nerve. 2021 Sep;64(3):346-351. DOI: 10.1002/mus.27344.

10- Filippini N, Douaud G, Mackay CE, et al. Corpus callosum involvement is a consistent feature of amyotrophic lateral sclerosis. Neurology. 2010 Nov 2;75(18):1645-52. DOI: 10.1212/WNL.0b013e3181fb84d1.

11- Winhammar JM, Rowe DB, Henderson RD, et al. Assessment of disease progression in motor neuron disease. Lancet Neurol. 2005 Apr;4(4):229-38. DOI: 10.1016/S1474-4422(05)70042-9.

12- Gupta A, Nguyen TB, Chakraborty S, et al. Accuracy of Conventional MRI in ALS. Can J Neurol Sci. 2014 Jan;41(1):53-7. DOI: 10.1017/s0317167100016267.

13- Jin J, Hu F, Zhang Q, et al. Hyperintensity of the corticospinal tract on FLAIR: A simple and sensitive objective upper motor neuron degeneration marker in clinically verified amyotrophic lateral sclerosis. J Neurol Sci. 2016 Aug 15;367:177-83. DOI: 10.1016/j.jns.2016.06.005.

14- Kassubek J, Müller HP. Advanced neuroimaging approaches in amyotrophic lateral sclerosis: refining the clinical diagnosis. Expert Rev Neurother. 2020 Mar;20(3):237-249. DOI: 10.1080/14737175.2020.1715798.

15- Basaia S, Filippi M, Spinelli EG, et al. White Matter Microstructure Breakdown in the Motor Neuron Disease Spectrum: Recent Advances Using Diffusion Magnetic Resonance Imaging. Front Neurol. 2019 Mar 5;10:193. DOI: 10.3389/fneur.2019.00193.

16- Steinbach R, Gaur N, Roediger A, et al. Disease aggressiveness signatures of amyotrophic lateral sclerosis in white matter tracts revealed by the D50 disease progression model. Hum Brain Mapp. 2021 Feb 15;42(3):737-752. DOI: 10.1002/hbm.25258.

17- Müller HP, Agosta F, Riva N, et al. Fast progressive lower motor neuron disease is an ALS variant: A two-centre tract of interest-based MRI data analysis. Neuroimage Clin. 2017 Oct 14;17:145-152. DOI: 10.1016/j.nicl.2017.10.008.

18- Brettschneider J, Del Tredici K, Toledo JB, et al. Stages of pTDP-43 pathology in amyotrophic lateral sclerosis. Ann Neurol. 2013 Jul;74(1):20-38. DOI: 10.1002/ana.23937.

19- Grapperon AM, Ridley B, Verschueren A, et al. Quantitative Brain Sodium MRI Depicts Corticospinal Impairment in Amyotrophic Lateral Sclerosis. Radiology. 2019 Aug;292(2):422-428. DOI: 10.1148/radiol.2019182276.

20- Brooks BR, Miller RG, Swash M, et al. El Escorial revisited: revised criteria for the diagnosis of amyotrophic lateral sclerosis. Amyotroph Lateral Scler Other Motor Neuron Disord. 2000 Dec;1(5):293-9. DOI: 10.1080/146608200300079536.

21- Cedarbaum JM, Stambler N, Malta E, et al. The ALSFRS-R: a revised ALS functional rating scale that incorporates assessments of respiratory function. BDNF ALS Study Group (Phase III). J Neurol Sci. 1999 Oct 31;169(1-2):13-21. DOI: 10.1016/s0022-510x(99)00210-5.

22- Labra J, Menon P, Byth K, et al. Rate of disease progression: a prognostic biomarker in ALS. J Neurol Neurosurg Psychiatry. 2016 Jun;87(6):628-32. DOI: 10.1136/jnnp-2015-310998.

23- Nagel AM, Laun FB, Weber MA, et al. Sodium MRI using a density-adapted 3D radial acquisition technique. Magn Reson Med. 2009 Dec;62(6):1565-73. DOI: 10.1002/mrm.22157.

24- Ridley B, Marchi A, Wirsich J, et al. Brain sodium MRI in human epilepsy: Disturbances of ionic homeostasis reflect the organization of pathological regions. Neuroimage. 2017 Aug 15;157:173-183. DOI: 10.1016/j.neuroimage.2017.06.011.

25- Avants BB, Tustison NJ, Stauffer M, et al. The Insight ToolKit image registration framework. Front Neuroinform. 2014 Apr 28;8:44. DOI: 10.3389/fninf.2014.00044.

26- Manjón JV, Coupé P, Concha L, et al. Diffusion weighted image denoising using overcomplete local PCA. PLoS One. 2013 Sep 3;8(9):e73021. DOI: 10.1371/journal.pone.0073021.

27- Jenkinson M, Beckmann CF, Behrens TE, et al. FSL. Neuroimage. 2012 Aug 15;62(2):782-90. DOI: 10.1016/j.neuroimage.2011.09.015.

28- Smith SM, Jenkinson M, Johansen-Berg H, et al. Tract-based spatial statistics: voxelwise analysis of multi-subject diffusion data. Neuroimage. 2006 Jul 15;31(4):1487-505. DOI: 10.1016/j.neuroimage.2006.02.024.

29- Bede P, Iyer PM, Schuster C, et al. The selective anatomical vulnerability of ALS: 'disease-defining' and 'disease-defying' brain regions. Amyotroph Lateral Scler Frontotemporal Degener. 2016 Oct-Nov;17(7-8):561-570. DOI: 10.3109/21678421.2016.1173702.

30- Steinbach R, Prell T, Gaur N, et al. Patterns of grey and white matter changes differ between bulbar and limb onset amyotrophic lateral sclerosis. Neuroimage Clin. 2021;30:102674. DOI: 10.1016/j.nicl.2021.102674.

31- Sach M, Winkler G, Glauche V, Liepert J, Heimbach B, Koch MA, Büchel C, Weiller C. Diffusion tensor MRI of early upper motor neuron involvement in amyotrophic lateral sclerosis. Brain. 2004 Feb;127(Pt 2):340-50. DOI: 10.1093/brain/awh041.

32- Chapman MC, Jelsone-Swain L, Johnson TD, et al. Diffusion tensor MRI of the corpus callosum in amyotrophic lateral sclerosis. J Magn Reson Imaging. 2014 Mar;39(3):641-7. DOI: 10.1002/jmri.24218.

33- Zhang F, Chen G, He M, et al. Altered white matter microarchitecture in amyotrophic lateral sclerosis: A voxel-based meta-analysis of diffusion tensor imaging. Neuroimage Clin. 2018 Apr 4;19:122-129. DOI: 10.1016/j.nicl.2018.04.005.

34- Huhn K, Engelhorn T, Linker RA, et al. Potential of Sodium MRI as a Biomarker for Neurodegeneration and Neuroinflammation in Multiple Sclerosis. Front Neurol. 2019 Feb 11;10:84. DOI: 10.3389/fneur.2019.00084.

35- Schuster C, Hardiman O, Bede P. Survival prediction in Amyotrophic lateral sclerosis based on MRI measures and clinical characteristics. BMC Neurol. 2017 Apr 17;17(1):73. DOI: 10.1186/s12883-017-0854-x.

36- Spinelli EG, Riva N, Rancoita PMV, et al. Structural MRI outcomes and predictors of disease progression in amyotrophic lateral sclerosis. Neuroimage Clin. 2020;27:102315. DOI: 10.1016/j.nicl.2020.102315.

37- Sassani M, Alix JJ, McDermott CJ, et al. Magnetic resonance spectroscopy reveals mitochondrial dysfunction in amyotrophic lateral sclerosis. Brain. 2020 Dec 1;143(12):3603-3618. DOI: 10.1093/brain/awaa340.

38- Vandoorne T, De Bock K, Van Den Bosch L. Energy metabolism in ALS: an underappreciated opportunity? Acta Neuropathol. 2018 Apr;135(4):489-509. DOI: 10.1007/s00401-018-1835-x.

39- Stys PK, Waxman SG, Ransom BR. Ionic mechanisms of anoxic injury in mammalian CNS white matter: role of Na+ channels and Na(+)-Ca2+ exchanger. J Neurosci. 1992 Feb;12(2):430-9. DOI: 10.1523/JNEUROSCI.12-02-00430.1992.

40- Kapoor R, Davies M, Blaker PA, Hall SM, Smith KJ. Blockers of sodium and calcium entry protect axons from nitric oxide-mediated degeneration. Ann Neurol. 2003 Feb;53(2):174-80. DOI: 10.1002/ana.10443.

41- Meier JM, van der Burgh HK, Nitert AD, et al. Connectome-Based Propagation Model in Amyotrophic Lateral Sclerosis. Ann Neurol. 2020 May;87(5):725-738. DOI: 10.1002/ana.25706.

FIGURE LEGENDS

Figure 1. Example of fractional anisotropy (FA) and total sodium concentration (TSC) maps in a healthy control (top), a fast progressor ALS patient (middle) and a slow progressor ALS patient (bottom).

Figure 2. Significant clusters resulting from the comparison between ALS patients and HC using voxel-wise analysis of TSC (increased in ALS) and tract-based spatial statistics for FA (decreased in ALS) and for MD (increased in ALS). A, anterior; ALS, amyotrophic lateral sclerosis; FA, fractional anisotropy; HC, healthy controls, L, left; MD, mean diffusivity; S, superior; TSC, total sodium concentration.

Figure 3. Significant clusters resulting from the comparison between fast ALS progressors and HC using voxel-wise analysis for TSC (increased in Fast ALS) and tract-based spatial statistics for FA (decreased in Fast ALS) and MD (increased in Fast ALS). A, anterior; ALS, amyotrophic lateral sclerosis; FA, fractional anisotropy; HC, healthy controls; L, left; MD, mean diffusivity; S, superior; TSC, total sodium concentration.

Figure 4. Significant clusters resulting from the comparison between slow ALS progressors and HC using tract-based spatial statistics for FA (decreased in slow ALS). A, anterior; ALS, amyotrophic lateral sclerosis; FA, fractional anisotropy; HC, healthy controls; L, left; S, superior.

Supplementary Figure 1. Significant clusters resulting from the comparison between ALS patients and HC using voxel-wise analysis for TSC (increased in ALS) and tract-based spatial statistics for RD (increased in ALS). A, anterior; ALS, amyotrophic lateral sclerosis; HC, healthy controls; L, left; RD, radial diffusivity; S, superior; TSC, total sodium concentration.

Supplementary Figure 2. Significant clusters resulting from the comparison between fast ALS progressors and HC using voxel-wise analysis for TSC (increased in fast ALS) and tract-based spatial statistics for RD (increased in fast ALS) and AD (increased in fast ALS). A, anterior; AD, axial diffusivity; ALS, amyotrophic lateral sclerosis; HC, healthy controls; L, left; RD, radial diffusivity; S, superior; TSC, total sodium concentration.

Table 1. Demographic and clinical data.

	ALS	fast	slow	HC	p-value
Number	29	13	16	24	-
Age (years)	54.3 ± 10.2	56 ± 9.9	52.9 ± 10.6	51 ± 10.7	0.244[a+], 0.152[a#], 0.586[a*], 0.388[a=]
Gender	9F/20M	6F/7M	3F/13M	11F/13M	0.394[b+], 0.101[b#], 1.000[b*], 0.172[b=]
Disease duration (months)	18.8 ± 14.5	19.4 ± 13.9	18.4 ± 15.4	NA	-[+], -[#], -[*], 0.660[c=]
Site of onset					
Spinal	22 (6 UL, 16 LL)	10 (3 UL, 7 LL)	12 (3 UL, 9 LL)		
Bulbar	7 (1 LL)	3 (1 LL)	4 (0 LL)		
Revised El Escorial criteria					
Definite	7	7	0		
Probable	7	3	6		
Probable laboratory supported	6	1	5		
Possible	9	2	5		
Disease progression rate	0.84 ± 0.87	1.54 ± 0.93	0.27 ± 0.09	-	-[+], -[#], -[*], **0.001**[c=]
ALSFRS-R (/48)	38.72 ± 5.55	37.31 ± 4.81	40.46 ± 6.09	-	-[+], -[#], -[*], 0.067[c=]

Values are expressed in mean ± SD.

ALSFRS-R. revised ALS functional rating scale; DD. Disease duration; F. female; fast, fast progressors; LL. lower limb; M. male; slow, slow progressors. NA. not applicable; UL. upper limb.

[a] Student's t-test; [b] Chi-squared test; [c] Kruskal-Wallis test

[+] ALS vs HC; [#] fast vs HC; [*] slow vs HC; [=] fast vs slow.

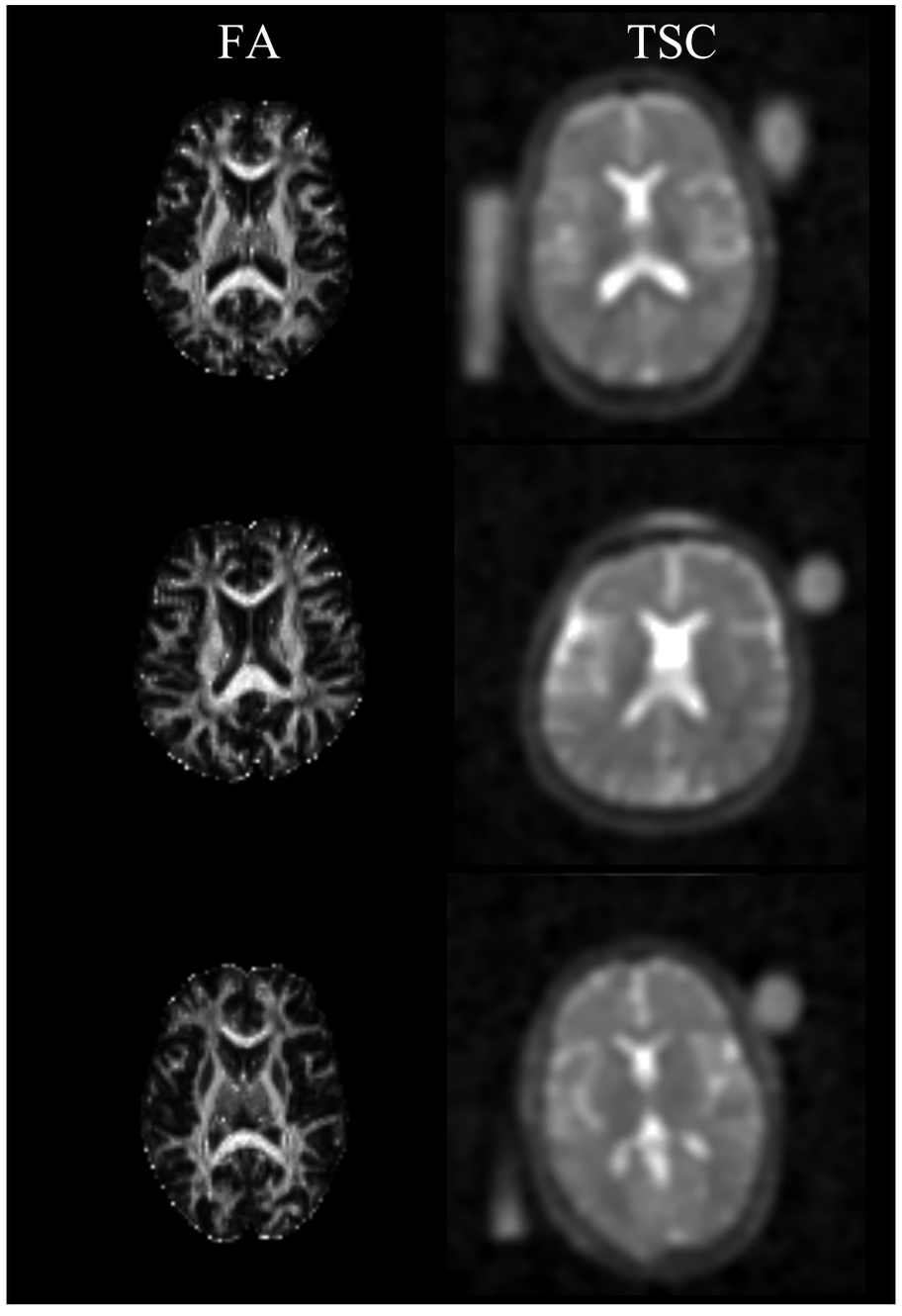


Figure 1.

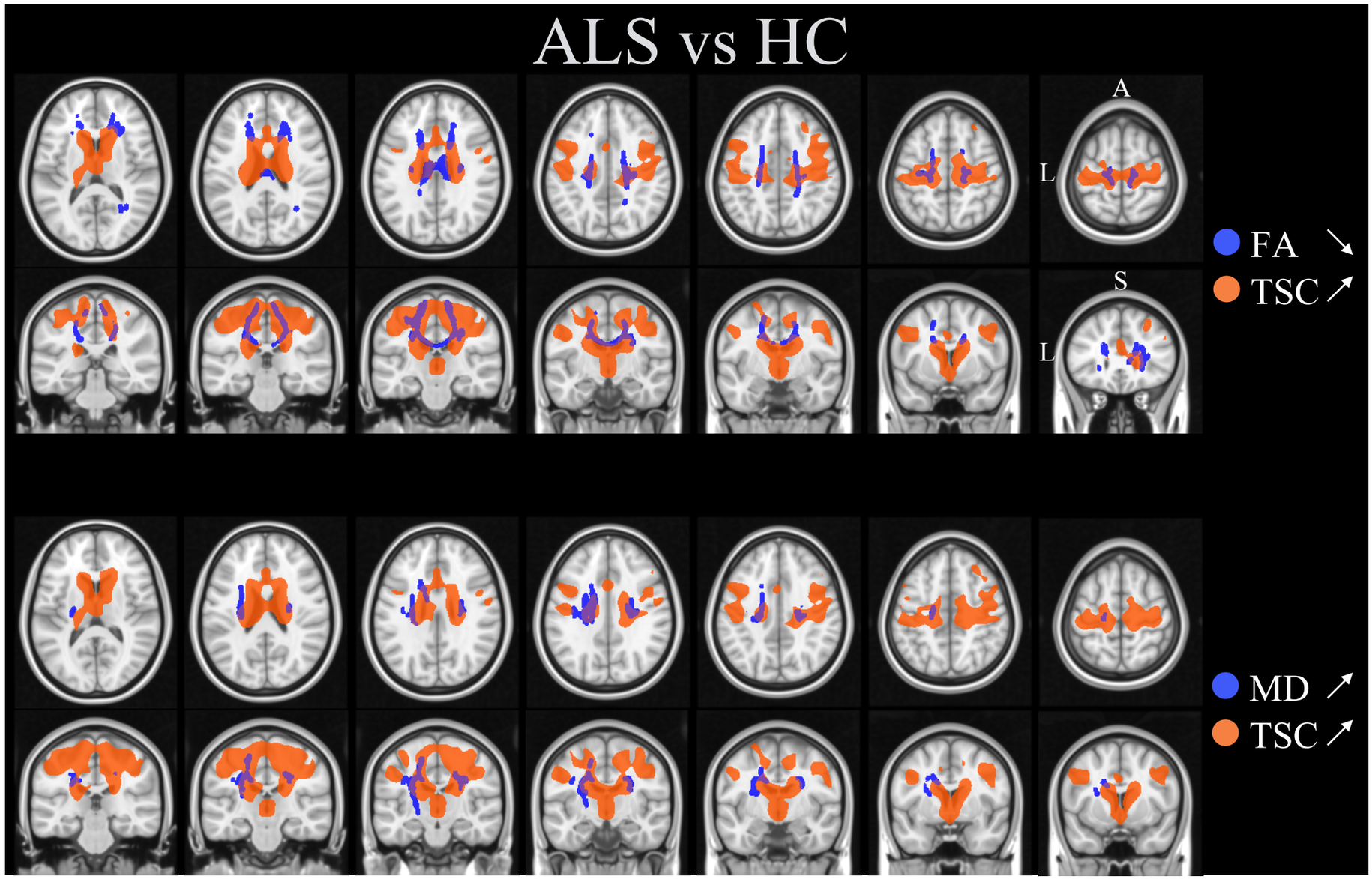


Figure 2.

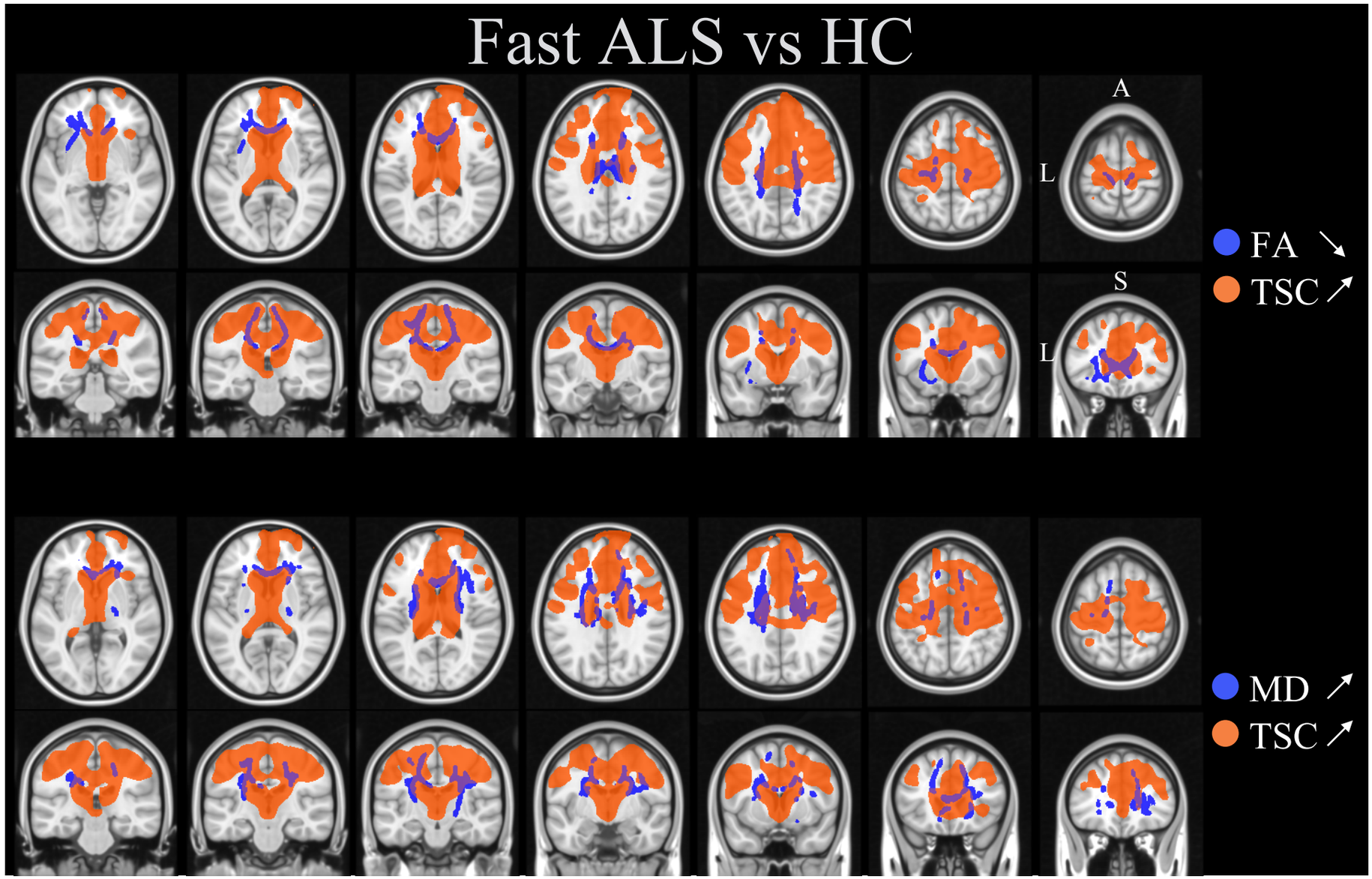


Figure 3.

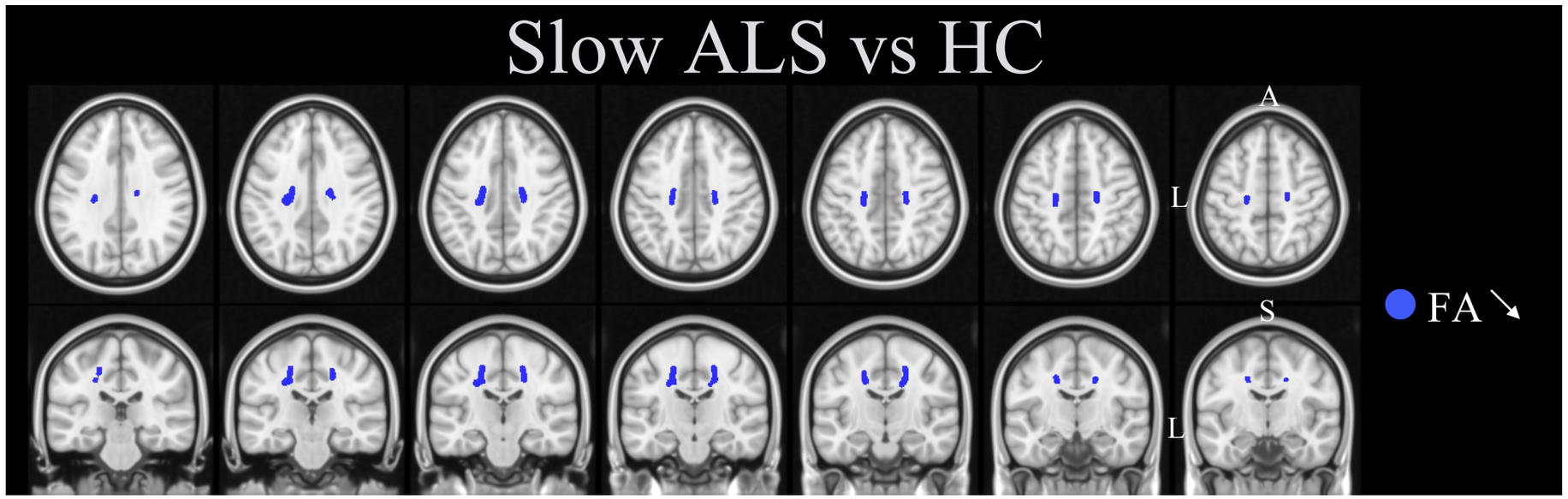
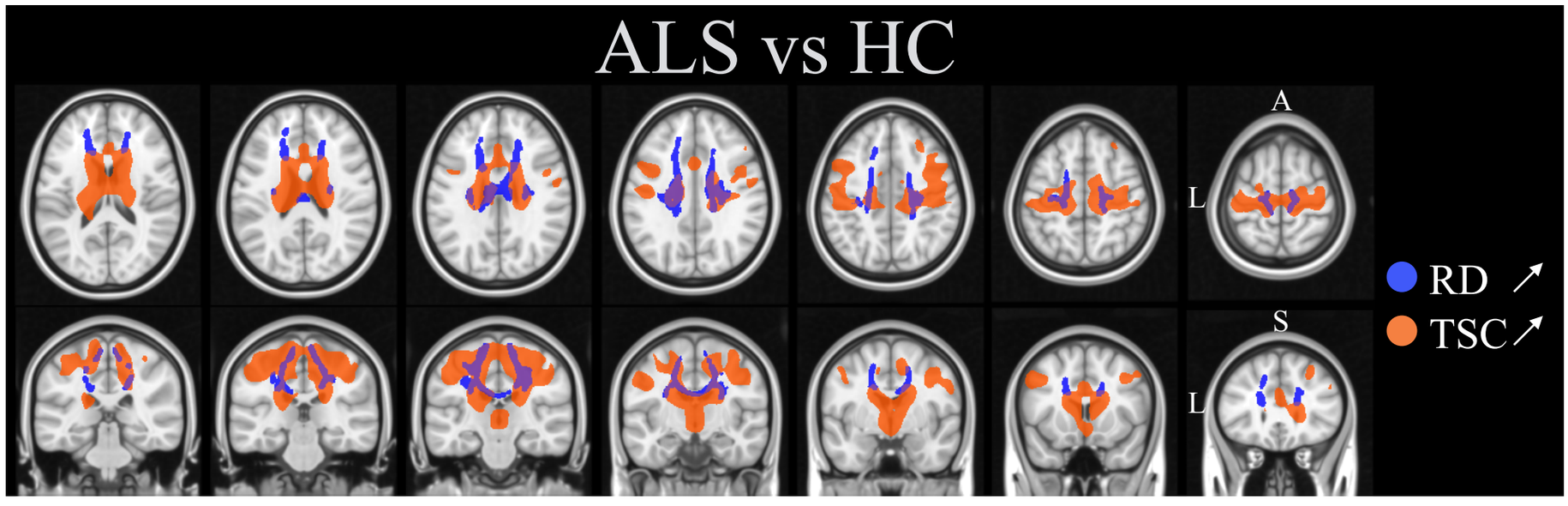
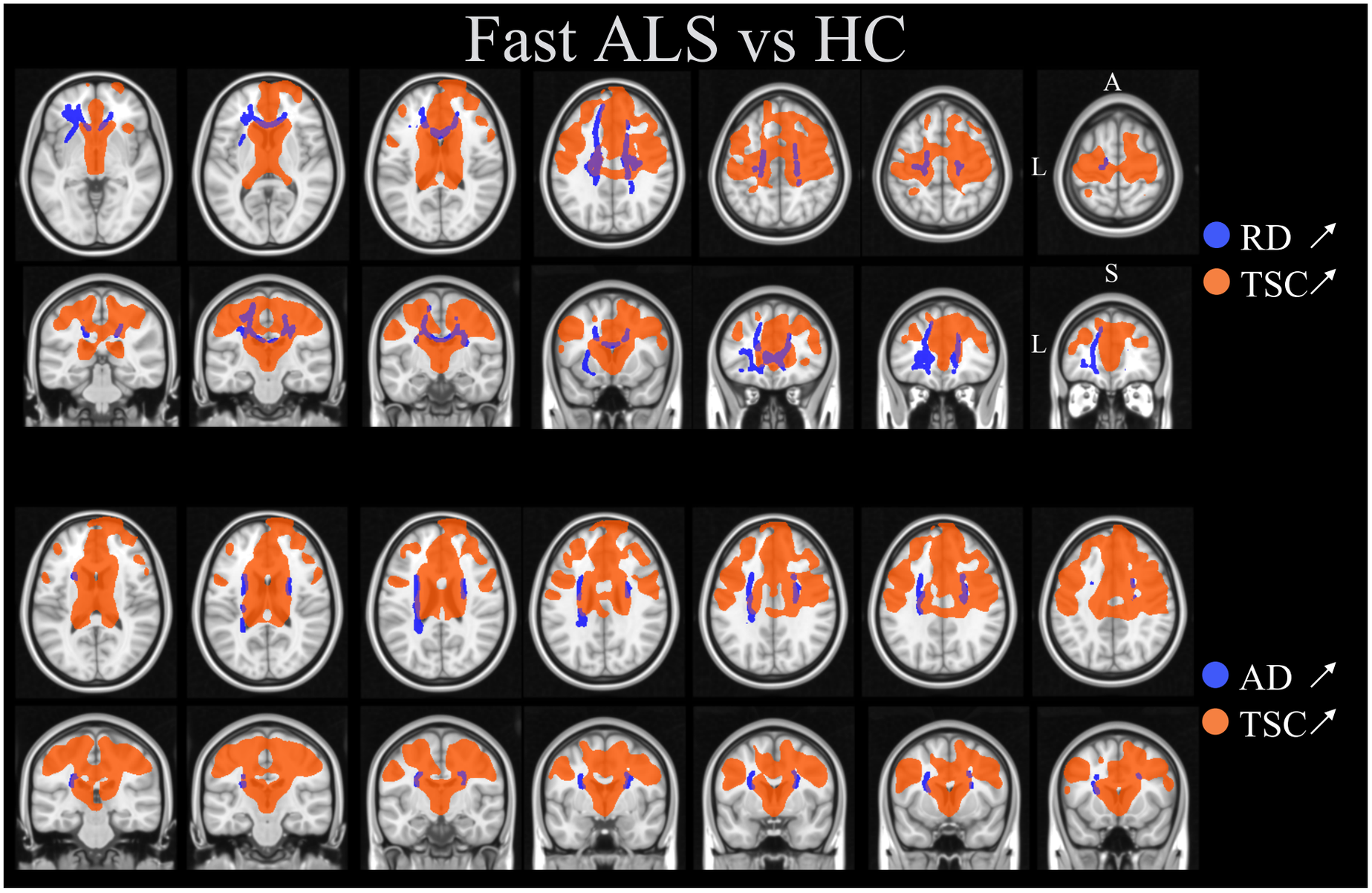


Figure 4.



Supplementary Figure 1.



Supplementary Figure 2.

Supplementary Table 1. Anatomic location of statisticaly significant regions revealed by voxel-wise analysis for total sodium comcentration (TSC), fractional anisotropy (FA), mean diffusivity (MD), radial diffusivity (RD) and axial diffusivity (AD) in ALS patients, Fast progressors, slow progressors, compared to healthy controls.

	Cluster size	Minimal p-value		MNI coordinates		
		DTI	TSC	X	Y	Z
ALS versus HC						
TSC ∩ FA						
Body of corpus callosum, superior corona radiata left, corticospinal tract left, posterior corona radiata left.	1584	0.036	0.048	-20	-20	37
Body of corpus callosum, superior corona radiata right, corticospinal tract right, genu of corpus callosum, posterior corona radiata right, Superior longitudinal fasciculus right, forceps minor, superior longitudinal fasciculus right, splenium of corpus callosum.	1565	0.024	0.048	16	-16	34
Body of corpus callosum, genu of corpus callosum, forceps minor.	60	0.047	0.042	-17	25	18
Anterior corona radiata right, anterior thalamic radiation right, Inferior fronto-occipital fasciculus right.	33	0.015	0.046	22	31	7
Inferior fronto-occipital fasciculus right, anterior corona radiata right.	19	0.044	0.048	24	28	1
Genu of corpus callosum, forceps minor.	13	0.044	0.048	14	31	8
Unclassified.	7	0.047	0.040	-24	-20	44

Inferior fronto-occipital fasciculus right, anterior corona radiata right.	2	0.036	0.040	25	27	9
Unclassified	1	0.039	0.036	16	3	51
Body of corpus callosum.	1	0.039	0.034	14	-8	35
Body of corpus callosum.	1	0.019	0.034	11	-3	29
Body of corpus callosum.	1	0.005	0.028	19	17	25
Genu of corpus callosum, forceps minor.	1	0.003	0.029	10	29	8
TSC ∩ MD						
Superior corona radiata left, corticospinal tract left, body of corpus callosum, posterior corona radiata left.	737	0.027	0.048	-24	-20	33
Superior corona radiata right, corticospinal tract right, Superior longitudinal fasciculus right, superior longitudinal fasciculus right.	311	0.050	0.044	24	-13	32
Posterior limb of internal capsule left, corticospinal tract left.	28	0.049	0.046	-26	-19	15
Body of corpus callosum.	20	0.030	0.033	-16	8	28
Superior corona radiata left, posterior limb of internal capsule left, corticospinal tract left.	16	0.049	0.033	-22	-11	18
Superior corona radiata right.	1	0.028	0.033	25	-13	35
Superior corona radiata left.	1	0.032	0.029	-30	-19	26
Superior corona radiata left.	1	0.023	0.029	-26	-9	24
TSC ∩ RD						

Superior corona radiata right, body of corpus callosum, corticospinal tract right, Superior longitudinal fasciculus right, superior longitudinal fasciculus right, posterior corona radiata right, genu of corpus callosum, forceps minor, splenium of corpus callosum.	1771	0.048	0.048	19	-18	36
Superior corona radiata left, body of corpus callosum, corticospinal tract left, posterior corona radiata left.	1599	0.047	0.048	-24	-22	34
Body of corpus callosum.	31	0.037	0.046	-16	10	27
Unclassified.	18	0.046	0.036	17	-3	46
Genu of corpus callosum, forceps minor.	17	0.046	0.048	-17	25	18
Unclassified.	9	0.047	0.042	-24	-20	44
Unclassified.	7	0.049	0.044	-35	-24	39
Body of corpus callosum.	3	0.049	0.044	-16	17	24
Body of corpus callosum.	1	0.041	0.046	14	-8	35
Body of corpus callosum.	1	0.040	0.044	13	-6	34
Body of corpus callosum.	1	0.040	0.038	11	3	28
Body of corpus callosum.	1	0.048	0.038	19	15	26
Body of corpus callosum.	1	0.033	0.035	19	17	25
Body of corpus callosum.	1	0.035	0.042	-16	14	25
Genu of corpus callosum.	1	0.034	0.033	-17	20	22
Genu of corpus callosum, forceps minor.	1	0.007	0.029	16	31	14
Genu of corpus callosum, forceps minor.	1	0.009	0.028	17	32	12
Fast versus HC						
TSC ∩ FA						

Body of corpus callosum, genu of corpus callosum, forceps minor, superior corona radiata right, superior corona radiata left, corticospinal tract left, anterior corona radiata right, corticospinal tract right, posterior corona radiata right, posterior corona radiata left, anterior corona radiata left, splenium of corpus callosum.	4334	0.031	0.049	-18	-20	34
Genu of corpus callosum, forceps minor.	20	0.040	0.049	-12	25	-6
Superior corona radiata left, corticospinal tract left.	13	0.032	0.049	-26	-20	32
Body of corpus callosum.	8	0.023	0.049	8	-27	24
Body of corpus callosum.	5	0.019	0.044	11	-25	26
Unclassified.	5	0.040	0.044	-8	16	-8
Body of corpus callosum.	4	0.032	0.035	9	-7	28
Body of corpus callosum.	1	0.040	0.041	10	-20	26
Body of corpus callosum.	1	0.040	0.041	7	-19	25
Body of corpus callosum.	1	0.019	0.024	8	-21	25
Genu of corpus callosum, forceps minor.	1	0.021	0.022	-13	29	-3
Genu of corpus callosum.	1	0.005	0.013	-12	22	-7
TSC ∩ MD						
Superior corona radiata right, body of corpus callosum, corticospinal tract right, Superior longitudinal fasciculus right, superior longitudinal fasciculus right, anterior corona radiata right, genu of corpus callosum.	1648	0.045	0.049	26	-12	30

Superior corona radiata left, body of corpus callosum, corticospinal tract left, posterior corona radiata left.	1114	0.024	0.026	-24	-20	33
Genu of corpus callosum, forceps minor, body of corpus callosum, anterior corona radiata right.	752	0.044	0.049	-4	28	6
Anterior limb of internal capsule right, superior fronto-occipital fasciculus (could be a part of anterior internal capsule) right, superior corona radiata right, posterior limb of internal capsule right, anterior thalamic radiation right, corticospinal tract right.	164	0.040	0.049	23	0	18
Anterior limb of internal capsule left, superior corona radiata left, anterior corona radiata left, superior fronto-occipital fasciculus (could be a part of anterior internal capsule) left, anterior thalamic radiation left, external capsule left.	136	0.045	0.044	-23	-1	19
Inferior fronto-occipital fasciculus right, anterior corona radiata right, anterior limb of internal capsule right, anterior thalamic radiation right.	110	0.040	0.049	23	26	0
Genu of corpus callosum, anterior corona radiata left, body of corpus callosum, superior corona radiata left.	62	0.045	0.049	-19	12	27
Unclassified.	46	0.043	0.035	15	10	47
Anterior corona radiata right, anterior thalamic radiation right, Inferior fronto-occipital fasciculus right.	45	0.021	0.049	25	28	10

Anterior corona radiata right, superior corona radiata right, anterior limb of internal capsule right.	41	0.045	0.049	25	15	16
Superior corona radiata right, anterior corona radiata right.	39	0.041	0.049	23	16	28
Body of corpus callosum.	21	0.039	0.041	-9	-24	26
Posterior limb of internal capsule left, superior corona radiata left.	20	0.043	0.044	-23	-11	17
Unclassified.	14	0.041	0.044	18	28	30
Anterior corona radiata right.	7	0.040	0.049	25	21	16
Body of corpus callosum.	5	0.041	0.049	-15	15	24
Posterior limb of internal capsule left, corticospinal tract left.	5	0.043	0.038	-26	-16	17
Anterior corona radiata left, anterior thalamic radiation left, Inferior fronto-occipital fasciculus left.	4	0.048	0.028	-24	19	12
Genu of corpus callosum.	3	0.017	0.038	20	23	22
Genu of corpus callosum, forceps minor.	3	0.045	0.016	-11	31	4
Superior corona radiata right.	2	0.036	0.049	29	-12	23
Inferior fronto-occipital fasciculus right, anterior corona radiata right.	2	0.041	0.038	25	25	13
Genu of corpus callosum, forceps minor.	2	0.030	0.013	-13	31	8
Inferior fronto-occipital fasciculus right, anterior corona radiata right.	2	0.041	0.033	21	25	-3
Superior corona radiata left.	1	0.038	0.031	-19	0	32

Unclassified.	1	0.036	0.031	18	28	28
Superior corona radiata left.	1	0.035	0.021	-19	10	28
Body of corpus callosum.	1	0.049	0.015	-16	16	26
Unclassified.	1	0.029	0.016	-17	38	24
Superior corona radiata right.	1	0.036	0.024	25	7	24
Body of corpus callosum.	1	0.018	0.013	6	10	22
Superior corona radiata right.	1	0.033	0.015	25	8	21
Anterior thalamic radiation right, anterior corona radiata right.	1	0.035	0.016	23	31	18
Corticospinal tract left, posterior limb of internal capsule left.	1	0.016	0.013	-26	-21	17
Forceps minor, anterior corona radiata right.	1	0.014	0.013	18	34	9
TSC ∩ RD						
Body of corpus callosum, genu of corpus callosum, forceps minor, superior corona radiata right, superior corona radiata left, corticospinal tract left, corticospinal tract right, anterior corona radiata right, posterior corona radiata right, posterior corona radiata left, anterior corona radiata left, Superior longitudinal fasciculus right, superior longitudinal fasciculus right, splenium of corpus callosum.	4113	0.029	0.049	-18	-15	34
Superior corona radiata left, corticospinal tract left, posterior corona radiata left.	93	0.041	0.041	-26	-19	32
Unclassified.	72	0.049	0.049	-11	42	35

Unclassified.	12	0.031	0.049	-12	31	41
Unclassified.	8	0.037	0.049	-17	38	24
Genu of corpus callosum, forceps minor.	7	0.031	0.049	-12	31	8
Unclassified.	7	0.029	0.044	-8	17	-8
Body of corpus callosum.	4	0.023	0.049	9	-10	27
Unclassified.	3	0.037	0.049	-15	37	30
Unclassified.	3	0.041	0.049	18	28	30
Body of corpus callosum.	3	0.041	0.049	5	-20	24
Body of corpus callosum.	2	0.049	0.044	-13	-23	28
Body of corpus callosum.	2	0.037	0.049	9	-13	27
Superior corona radiata right.	2	0.041	0.049	29	-13	23
Unclassified.	1	0.020	0.049	15	-38	38
Unclassified.	1	0.041	0.044	-13	37	34
Unclassified.	1	0.031	0.044	-13	42	30
Unclassified.	1	0.037	0.044	-14	40	30
Unclassified.	1	0.032	0.044	18	28	28
Superior corona radiata left.	1	0.041	0.044	-19	10	28
Body of corpus callosum.	1	0.029	0.035	10	-20	26
Body of corpus callosum.	1	0.049	0.035	7	-19	25
Body of corpus callosum.	1	0.032	0.044	8	-21	25
Genu of corpus callosum.	1	0.041	0.035	-16	22	24
Unclassified.	1	0.041	0.022	0	-21	23

Anterior corona radiata left.	1	0.017	0.013	-25	14	13
Genu of corpus callosum.	1	0.007	0.013	-12	22	-7
TSC ∩ AD						
Superior corona radiata right.	201	0.033	0.049	25	-5	23
Superior corona radiata left, posterior corona radiata left.	162	0.045	0.049	-27	-9	27
Anterior corona radiata left, anterior limb of internal capsule left, anterior thalamic radiation left, superior corona radiata left, external capsule left.	70	0.039	0.049	-23	0	19
Superior corona radiata right, superior fronto-occipital fasciculus (could be a part of anterior internal capsule) right.	23	0.033	0.022	24	0	20
Posterior corona radiata left.	22	0.016	0.024	-21	-30	28
Superior corona radiata right.	1	0.012	0.013	25	4	28
Superior corona radiata right.	1	0.013	0.013	25	8	21
Superior corona radiata right.	1	0.013	0.014	25	9	19
Slow versus HC						
FA						
Superior corona radiata left, corticospinal tract left.	199	0.039	-	-21	-21	38
Superior corona radiata right, body of corpus callosum, corticospinal tract right.	120	0.036	-	20	-18	38